Carpathian Journal of Earth and Environmental Sciences, September 2011, Vol. 6, No. 2, p. 235 - 249

ISOTOPE GEOCHEMISTRY OF THE SHIHU GOLD DEPOSIT, HEBEI PROVINCE, NORTH CHINA: IMPLICATION FOR THE SOURCE OF ORE FLUID AND MATERIALS

Ye CAO[1,2], Shengrong LI[1], Meijuan YAO[1,2], Huafeng ZHANG[1], Shaoqing JIANG[3] & Huapeng NIU[4]

[1]*State Key Laboratory of Geological Processes and Mineral Resources, China University of Geosciences, Beijing 100083, China*

[2]*Department of Earth Sciences, Laurentian University, Sudbury P3E2C6, Canada.*

[3]*Chinese Academy of Geological Sciences, Beijing 100037, China*

[4]*China University of Petroleum, Beijing 102249, China*

Corresponding author: cykaiyang@yahoo.com.cn

Abstract: The Shihu deposit, which is a well known quartz vein type gold deposit in the northern part of the Taihang orogen of the North China craton (NCC), is hosted by ductile-brittle faults within Archean metamorphic core complex of the Fuping Group. Lead, sulfur, carbon, oxygen, hydrogen and strontium isotope geochemistry is used to help understand the sources of the ore fluid and materials. Pb isotopic compositions from sulfides range from 16.002-16.958 for $^{206}Pb/^{204}Pb$, 15.134-15.345 for $^{207}Pb/^{204}Pb$, and 36.825-37.8194 for $^{208}Pb/^{204}Pb$. The data straddle the lower crust and upper mantle growth curve. These values are similar to those of country rocks, and indicate that there are mixed sources for the Pb, with end members equating to mantle and crustal reservoirs. Most $\delta^{34}S$ values of the sulfides range from +1.5 to +2.5 ‰ and display a pronounced tower effect, and suggest that magmatic sulfur dominates in sulfides, mixed with minor, isotopically light sulfur. Sulfur isotope temperatures calculated by mineral pairs are between 160□ and 315□. Gangue calcite in three samples from the veins have similar isotope compositions, with $\delta^{13}C$ values in the range of -5.93 to -6.92 ‰ with respect to PDB and $\delta^{18}O$ values in the range of 8.81 to 12.36 ‰ with respect to SMOW. δD values of fluid inclusions in the seven samples of auriferous quartz have a narrow range of -101 to -91 ‰ and the $\delta^{18}O_{H2O}$ values calculated from $\delta^{18}O$ values of quartz range from 2.21 to 7.05 ‰. These data suggest that the ore fluid is likely a mixture of meteoric water and magmatic water. The initial $^{87}Sr/^{86}Sr$ values range from 0.714057 to 0.825903 for quartz, from 0.71345 to 0.723227 for pyrite, which are lower than that of the host rock ranging from 0.77569 to 1.06413. Those results suggest that the ore-forming elements were leached from the Precambrian basement that reacted with deep-source fluids.

Key words: isotope geochemistry, sources of ore fluid and materials, Shihu gold deposit, North China craton.

1. INTRODUCTION

Previous studies of gold deposits have been focused on the major gold-bearing areas along the margin of the North China craton (NCC), such as Jiaodong peninsula (eastern margin), Xiaoqinling (southern margin), and Chifeng-Chaoyang (northern margin) (Yang et al., 2003); however, gold deposits within the NCC are still poorly studied (Zhu et al., 2001). As a polymetallic metallogenic province, the Taihang Mountain, associated with the NE-SW trending giant gravity lineament (NSGL), is an ideal probe of studying destruction of the NCC (Chen et al., 2003, 2005, 2008). Recent exploration has targeted gold deposits in the Taihang Mountains that are associated with granitoids and more than 88 gold deposits and occurrences have been found (Yang et al., 1991). Their economic importance, total contained gold (production and reserves) exceeding 100 tons of gold, has made them the targets of many investigations. The largest old

gold deposit in this area is the Shihu mine, which was first discovered in 1980s, and still has reserves of more than 10 tons of gold with a grade of 6-14 grams per ton (Xi et al., 2008; Cao et al., 2010, 2011).

Geochemistry of ore fluid and metals of gold deposit from the Taihang Mountains have been systematically presented in one English language journals (Zhu et al., 2001), but those data not involved the Shihu deposit and lacked detailed new isotopic data. Many aspects of the ore genesis, such as the sources of metal, nature of the transporting fluids, and precipitating mechanisms are still matters of debate, either they were formed in the host rocks by hydrothermal processes preceding granitoid emplacement or there is no genetic relation with the younger plutonic rocks. Isotope geochemistry is a powerful tool in deciphering the genesis of ore deposits (Constantina et al., 2009; Andras et al., 2010). Hydrogen, oxygen and carbon isotope systems (Hoefs, 1997) can trace the sources of the ore-forming fluids and lead, sulfur, lead and strontium (Robert et al., 2001) and isotope analyses can constrain the source rocks for the ore-forming metals. We present new and detailed sulfur, hydrogen, oxygen, carbon, lead, and strontium isotope data in an attempt to constrain the sources of the ore fluid and metals of the Shihu gold field, and provide a valuable tool in the exploration for similar deposits in the region.

2. REGIONAL GEOLOGCAL SETTING

The North China craton (NNC, also known as the Sino-Korean craton), with basement rocks as old as 3.8 Ga is located in the eastern part of the Euro-Asian continent (Fig. 1a), bounded to the north by the southern margin of Inner Monglia-Daxing'anling orogen and to the south by the Qingling-Dabie-Sulu orogen that formed during the Triassic collision between the Yangtze Block and the NCC (Li et al., 1993). The Taihang Mountains, part of the NE-SW trending giant gravity lineament (NSGL) (Fig. 1b) was identified based on geophysical data (Ma, 1984) and is about 700km in SN length and 50-150km in EW breadth. According to some newly documented references, the Taihang Mountain is a special geomorphological-Tectonic unit within the North China craton which separates the Ordos cratonic block in the west and the North China quasi-circular rift basin in the east (Menzies et al. 2007). The region to the west of the NSGL shows large negative Bouguer gravity anomalies and is underlain by a thick (150-220 km) lithospheric mantle; the region to the east of the NSGL, however, shows weakly negative to positive Bouguer gravity anomalies and high heat flow and is underlain by a relatively thin lithosphere (60-120 km) (Tang et al., 2006). Extensive Mesozoic magmatism, together with the development of large-scale sedimentary basins, occurs mainly in the region east of the NSGL, contrasting to minor magmatism in the region west of the gravity lineament.

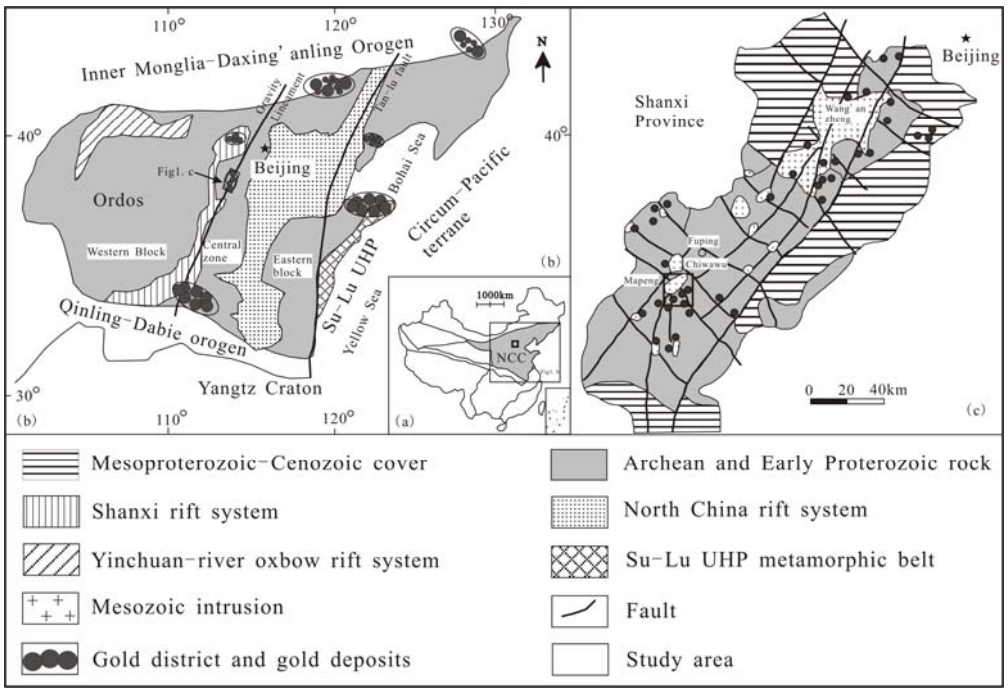

Figure 1. Skeleton geological map of the North China craton (left) and the Shihu region (right), western Hebei (Modified by Niu et al, 1994 and Tang et al, 2006).

The Taihang Mountain lies between the Ordos-Shanxi plateau to the west and the North China Basin to the east (Fig. 1b). The base of Taihang belt consist mainly of Archean TTG gneiss, which are uncomfortably overlain by thick sequences of Meso- to Neoproterozoic clastic and chemical sedimentary rocks, suggesting that craton was stabilized during Paleoproterozoic. The craton was stable until late Triassic when widespread volcanism (predominantly basaltic, andesitic and dacitic rocks, with minor rhyolites) and intrusion of dominantly intermediate to felsic plutons occurred, accompanied by large-scale basin formation. The Mesozoic magmatism continued intermittently until late Cretaceous, and resulted in the NE-trending magmatic belts in East China (Zhai et al., 2002). Voluminous Mesozoic intrusions occur in the orogen, with rock types dominated by monzonites-monzogranites and related mafic rocks. Chen et al. (2008) reported SHRIMP zircon U-Pb ages of 127±3 Ma and 129±3 Ma for a quartz monzonite pluton and a monzonite pluton in the orogen, respectively. An older age of 138±2 Ma was also reported by Chen et al. (2005) for a mafic pluton from the orogen.

3. DEPOSIT GEOLOGY

The Shihu gold district, about 200km southwest of Beijing, is situated with maximum reserves in the Long Mengou village, north-western Lingshou County, Shijiazhuang, the capital of Hebei province (Fig. 1c). The geographic coordinates of the deposit is 114°03′15″E—114°04′21″E and 38°38′04″N—38°40′19″N, with a total mine area of about 4.1km^2.

The deposit is a typical quartz vein type gold system with quartz-sulfide veinlets. Wall rocks consist of metamorphosed Precambrian sequences, which consist of 2.5~2.4Ga tonalite-trondhjemite-granodiorite (TTG) gneisses tectonically flattened and display well-developed foliations, ~2.5Ga Wanzi paragneisses that are mainly derived from aluminous schist and gneisses with minor amounts of calc-silicate rocks, marbles and amphibolites, and ~2.0Ga Nanying granitic gneisses, commonly containing the TTG as xenoliths, which are mainly derived form monzogranitic and syenogranitic varieties (Liu, 1997; Liu et al., 2004). All of them are metamorphosed to amphibolite to granulite facies.

The Mapeng granite batholith, with a total exposed area of about 64.5km^2, is one of the most important intrusions in the Shihu area. This stock intruded the Archean Fuping complex and is composed mainly of medium- to coarse grained massive granites. Small mafic enclaves (5-15 cm long) that have sharp contacts with the hosting granite are locally present. In addition, an NE-striking swarm of diorite and quartz diorite porphyry dikes intrude into the Archean Fuping complex, broadly parallel to the gold vines.

More than 50 quartz veins have been identified in the deposit, which trend SN and dip west or east (Fig. 2). These veins are generally 2m-5m in width and hundred of meters in length. The main lode is approximately up to 3200 m long and 2-5 m wide (locally up to 10 m), and has an average gold grade of 5.88g/t with a maximum grade of 100g/t (Fig. 3, Wang et al., 1990) In terms of paragenetic sequences, these gold-bearing veins can be divided into three types: (1) pyrite sericite-quartz veins; (2) disseminated pyrite veins; and (3) polymetallic sulfide veins. Type 1 veins were generally deformed, fractured and altered, and the homogenization temperatures of fluid inclusions in quartz of this type range from 350□ to 400□. Type 2 veins contain much less sericite and more pyrite than type 1. Type 2 veins locally crosscut type 1 veins, indicating that they are younger than type 1 veins, but both types crosscut the foliation of the host Archean gneiss. The homogenization temperatures of the type 2 veins vary between 300□ and 370□. Type 3 veins contain much more sulfide minerals than type 1 and type 2. The homogenization temperatures of this type change from 230□ to 310□. The type 2 and type 3 veins are economically significant, with ore grade generally ranging from 4.50 to 8.35 g/t (up to 100 g/t), whereas type 1 veins normally contain less than 1 g/t Au.

The alterations are mainly K-feldspathization, pyrite sericite-qyartz alteration, silicification as well as less carbonatization, sericitization, kaolinization, and chloritization. The intensive polymetallic sulfide and silicification are closely associated with gold mineralization. Ore structures commonly include automorphic granular structure (cubic pyrite in galena, Fig. 4c), inclusion structure (dendritic gold in quartz, Fig. 4a) and decomposition of solid solution structure (droplet chalcopyrite in sphalerite, Fig. 4d). According to ore textures, structures and mineral assemblages, ore-forming processes are divided into five stages: a pyrite phyllic stage (I), a coarse grain pyrite-milky white quartz stage (II), a smoky gray Au-bearing quartz-fine grain pyrite stage (III), an Au-bearing polymetallic sulfide-quartz stage (IV), and a quartz-carbonate stage (V). III and IV are the main ore-forming stages and the superposition of these two stages forms bonanza zones.

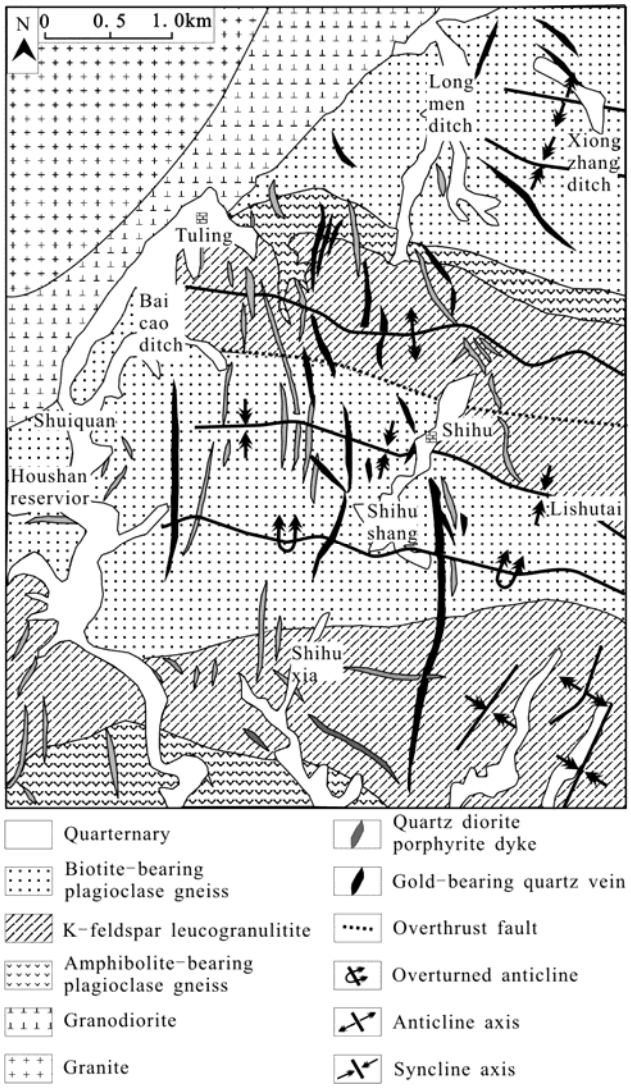

Figure 2. Mining geological map of Shihu gold mining area in western Hebei (Modified by Niu et al, 1994).

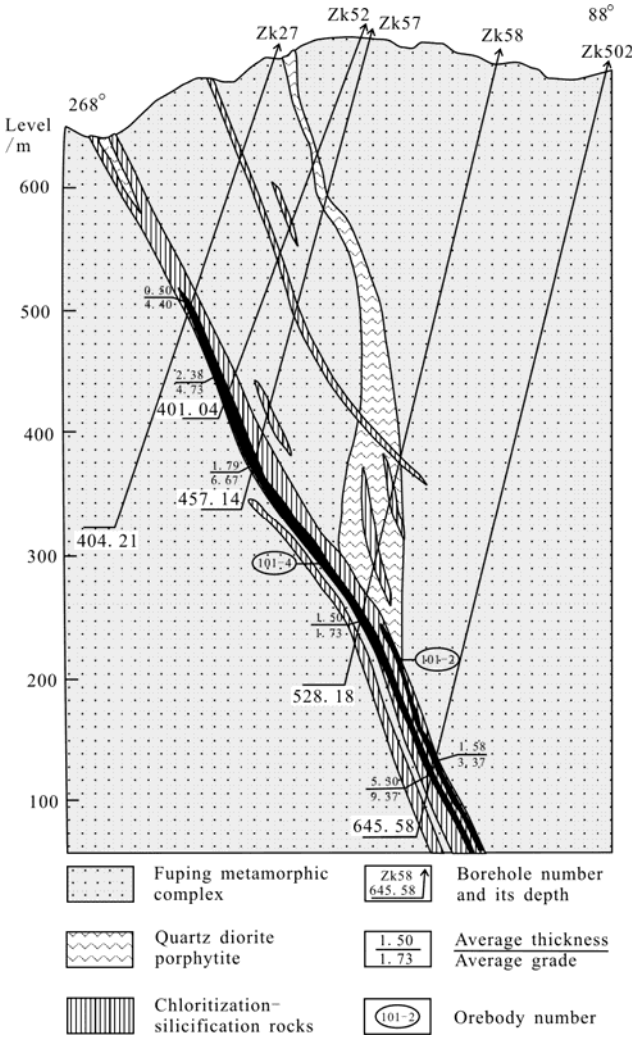

Figure 3. Profile of No. 23 exploration line of No.101 vein in the Shihu gold deposit, western Hebei (Modified by Wang et al., 1990).

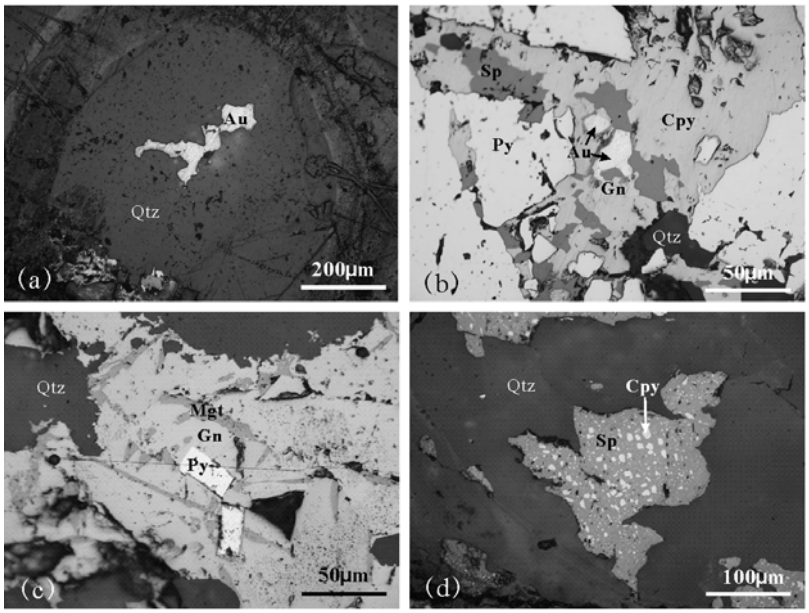

Figure 4. Reflected light photomicrographs showing ore mineral assemblage and textures of the Shihu gold deposit in western Hebei. Au=gold; Q=quartz; Gn=galena; Cpy=chalcopyrite; Py=pyrite; Mgt=magnetite; Sp=sphalerite.

The mineralogy of both type 1 and 2 gold-bearing veins is relatively simple, and sulfide minerals commonly comprise less than 5 percent of the vein materials. Pyrite, chalcopyrite, galena and sphalerite are the dominant sulfide and are accompanied by amounts of magnetite (Fig. 4c), with minor pyrrhotite, bornite and native ruthenium (Peng & Xu, 1994). Quartz and K-feldspar are the dominant gangue minerals, with subordinate sericite, carbonate, biotite and chlorite. Gold minerals, including native gold, electrum and kustelite, are mainly hosted within fractures and cracks developed in quartz (Fig. 4a) and polymetallic sulfide (Fig. 4b). The shape of gold minerals are typically spherulitic, flakes and dendritic.

4. SAMPLING AND METHOD

Only fresh samples of No. 101 orebody selected from underground working were prepared as polished thin-sections and polished blocks for ore microscopy and petrology. Individual minerals were extracted from the various ore veins and were lightly crushed to grain size of approximately 40 to 60 mesh using a carefully pre-cleaned agate mortar and pestle, washed and then handpicked to a purity of more than 99% under a binocular microscope.

Sulfur isotope analyses were carried out using 200-mesh pyrite, galena, sphalerite, and chalcopyrite. The samples were prepared for sulfur isotope analyses following the procedure as outlined by Glesemann et al (1994) and measurements were performed in a MAT-251EM mass spectrometer in the Stable Isotope Laboratories of China Academy of Geological Sciences (CAGS). Data are reported to an accuracy of ±0.2 ‰ (two standard deviations), relative to Vienna Canon Diablo Troilite (V-CDT) and a variety of secondary standards.

Together with the host rock and granitoid, lead isotope analyses were performed on single crystal of sulfide prepared for sulfur isotopic analysis. Lead-isotopic compositions were analyzed in static mode (simultaneous measurement of all isotopic ion currents) using a Finnigan MAT–262 thermal ionization multi-collector mass spectrometer at the Institute of Geology in CAGS. Carr et al. (1995) described the preparation of samples for lead isotope analyses at the CSIRO Exploration and Mining lead isotope laboratory at North Ryde, Sydney. Ratios were normalized to accept values of international standard NBS SRM 981, which are 2.1672±0.0003 for $^{208}Pb/^{206}Pb$, 0.91476±0.00023 for $^{207}Pb/^{206}Pb$, 16.9445±0.0096 for $^{206}Pb/^{204}Pb$, 15.4980±0.0077 for $^{207}Pb/^{204}Pb$, 36.7211±0.0217 for $^{208}Pb/^{204}Pb$, all have been demonstrated at the 2σ confidence level. Precision estimates representing two standard deviations are 0.05% for the $^{207}Pb/^{206}Pb$ ratio and 0.1% for all other ratios (Gulson et al. 1984).

Carbon and oxygen isotope compositions were determined on calcite. Carbonate gas extractions were carried out following the standard procedure of McCrea (1950). The reaction time for calcite is 4h using a thermostated water bath at 25□ (McCrea, 1950). The CO_2 was analyzed on a MAT 251 EM mass spectrometer at Chinese University of Geosciences. The reproducibility is better than 0.1 ‰ and 0.2 ‰ for carbon and oxygen, respectively. Carbon and oxygen isotope results are expressed as ‰ deviation from the PDB and SMOW, respectively.

Pure quartz separates were prepared for hydrogen and oxygen isotope analysis. The O-isotopic compositions of quartz were analyzed following the BrF5 method (Clayton & Mayeda, 1963). The $\delta^{18}O$ values were determined on a Finnigan MAT 252 ratio mass spectrometer at the Institute of Geology in CAGS. The δD values of water were analyzed using the Zn reduction method (Coleman et al., 1982). The H_2 and CH_4 from fluid inclusions were firstly converted to H_2O by passing through a CuO furnace at a temperature of 600□. Then, all H_2O were combined together and converted to H_2 by reacting with Zn in a vacuum line. The δD values were measured on the same mass spectrometer. The D/H ratios are expressed in the δD value in ‰ relative to V-SMOW. Reproducibilities of both $\delta^{18}O$ and δD are ±1 ‰. Oxygen isotopic compositions of hydrothermal waters in equilibrium with quartz were calculated using an extrapolation of the fractionation formula from Taylor (1974). The calculations of the fractionation factors were made using the mean value of the homogenization temperatures of fluid inclusions plus pressure-corrected temperatures.

Rb and Sr isotopic compositions of pyrite and quartz were analyzed at Institute of Geology and Geophysics, Chinese Academy of Sciences. Weighing ~500 mg pure pyrite and quartz grains were separately transferred to Teflon vessels, after being washed ultrasonically in millipore water, and dissolved using a mixture of HCl and HNO_3 in a ratio of 1:3. Subsample solutions were dried and redissolved in HCl for Rb, Sr, and loaded on quartz columns. Separation of the required elements for isotopic analysis was by cation exchange. Isotopic ratio measurements were made on a multicollector VG-354 thermal ionization mass spectrometer as described by Qiao (1988). Sr isotopic data were normalized to $^{86}Sr/^{88}Sr=0.1194$; the $^{87}Sr/^{86}Sr$ of the Sr standard NBS-607 during this study was 1.200393±12 (2σ, n=6). Errors are quoted

throughout as two standard deviations from measured or calculated values. Analytical uncertainties are estimated to be <0.5% for $^{87}Rb/^{86}Sr$ ratio. A fractionation correction of 0.1%/amu (atomic mass unit) was applied on the basis of analysis of standard NBS981. Blanks during the course of this study averaged 0.4 ng for Rb and 0.2 ng for Sr (Yang & Zhou, 2001).

5. RESULTS AND DISCUSSION

5.1 Lead isotopes

The Pb isotope compositions of single minerals of sulfide from mineralized zone, alteration zones and unmineralized country rock are listed in table 1. The lead isotopic compositions overlap the average lower crustal Pb evolution curves for uranogenic lead and thorogenic lead. The ratios of $^{206}Pb/^{204}Pb$, $^{207}Pb/^{204}Pb$, and $^{208}Pb/^{204}Pb$ for sulfide have a narrow range from 16.002-16.958, 15.134-15.345, and 36.825-37.8194, with mean values of 16.342, 15.249, and 37.236, respectively. This general isotopic consistency between ore and rocks is a feature that we interpret as evidence for a very local source control of lead in the sulfides (Ault et al., 2004, Andras et al., 2010).

As shown on plot of $^{207}Pb/^{204}Pb$ vs. $^{206}Pb/^{204}Pb$ diagram (Fig. 5b), the Pb isotope ratios of sulfides straddle the lower crust and upper mantle growth curves of Zartman & Haines (1988), demonstrating that the Pb reservoirs for both included a mixture of mantle and crustal sources. We attribute the least radiogenic values to a primitive, mantle-like continental margin mafic volcanic rock and the more radiogenic values were obtained from leaching of the evolved supracrustal rocks and trondhjemite-tonalite-granodiorite (TTG). On the other hand, in the $^{208}Pb/^{204}Pb$ vs. $^{206}Pb/^{204}Pb$ diagram (Fig. 5a), the majority data of the sulfide shows a linear trend along the lower crust growth curve. The wide variations in $^{208}Pb/^{204}Pb$ ratios, at a fairly narrow range of values of $^{206}Pb/^{204}Pb$, suggest lead mixing from various sources. The most likely interpretation is that the ore leads reflect mixtures of relatively unradiogenic (low U/Pb) and more radiogenic (high U/Pb) sources such as are typically found in geologically complex Paleoproterozoic collisional orogens (Zhao et al, 2000; Gülcan, 2009). Significantly, the primary igneous geochemistry of the Mesozoic plutonic rocks in the northern part of Taihang Mountain indicates mixing of mantle and crustal magmas (Chen et al, 2003, 2008).

Based on the single-stage evolution model of normal lead (Doe & Stancey, 1974), the calculated model ages for the sulfides exhibit a wide range from ~902 to ~1440Ma (isochron line age at about 2778Ma), μ and ω values are 8.9~9.32 and 38.5~46.1, with the mean values of 9.11 and 41.0, respectively, similar to those of the plutonic rocks and metamorphic rocks, which are 1110 and 842 Ma for Φ, 9.0 and 8.8 for μ, as well as 38.3 and 41.6 for ω. All of them suggest a source with a greater μ and ω values (Zhu, 1995) are mixed reservoirs for the Pb with end members equating to lower crust and upper mantle.

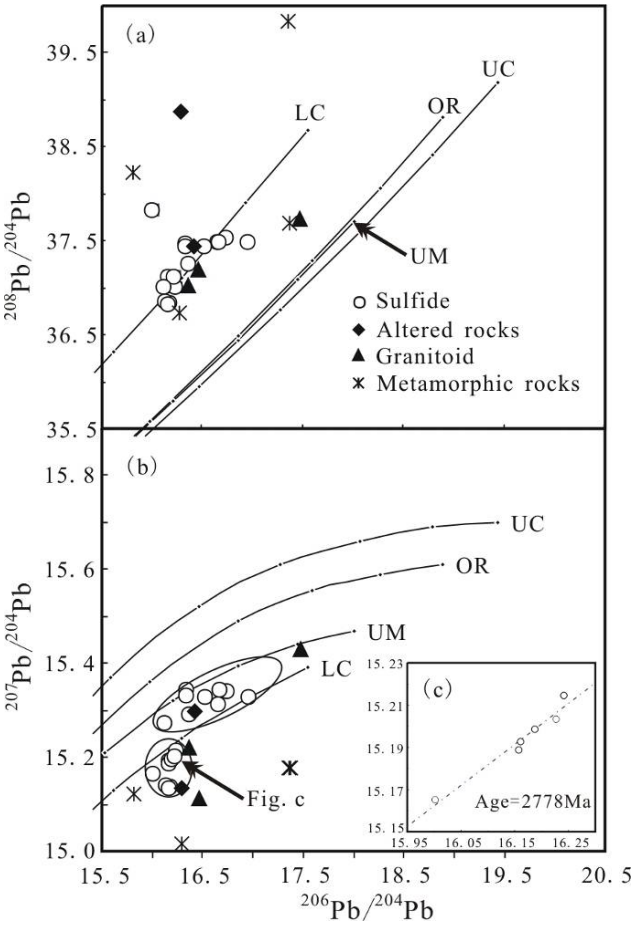

Figure 5 (a) Plot of $^{207}Pb/^{204}Pb$ vs. $^{206}Pb/^{204}Pb$ and $^{208}Pb/^{204}Pb$ vs. $^{206}Pb/^{204}Pb$, and (c) isochron line diagrams showing lead compositions of sulfides, altered rocks, granitoid, and metamorphic rocks from Shihu gold deposit. UC=upper crust; OR=orogenic belt; UM=upper mantle; LC=lower crust.

In the Δβ-Δγ classification diagram (Zhu, 1998) (Fig. 6) without time factors, the data for sulfides, granitoid and altered rocks plot within the area of middle to deep metamorphism (area 6) and orogenic belt (area 8), and these data are close to the boundary of area 6 and area 8, whereas the data for metamorphic rocks plot only within the area of middle to deep metamorphism (area 6). It suggests that lead sources for the deposit were derived from a mixture composed of Precambrian metamorphic complex and magmas related to the pluton.

Table 1. Lead isotopes compositions of sulfides, altered rocks, plutonic rocks, and metamorphic rocks from the Shihu gold deposit (an external reproducibility for lead isotopic ratios are 0.1% for $^{206}Pb/^{204}Pb$, 0.15% for $^{207}Pb/^{204}Pb$, and 0.2% $^{208}Pb/^{204}Pb$ at the 2σ confident level).

Sample no.	*Sample*	*Location*	$^{206}Pb/^{204}Pb$	$^{207}Pb/^{204}Pb$	$^{208}Pb/^{204}Pb$	*φ(Ma)*	*μ*	*ω*	□*α*	□*β*	□*γ*	*Reference*
560-13	pyrite	pyrite-quartz vein	16.16	15.193	37.026	1332	9.03	40.68	38.25	0.83	48.17	This study
220-9	pyrite		16.157	15.189	37.121	1330	9.02	41.17	37.85	0.52	50.76	
180-9	chalcopyrite	polymetallic sulfide quartz vein	16.002	15.165	37.819	1419	9.02	46.1	36.72	0.24	75.04	
300-25	chalcopyrite		16.187	15.199	37.019	1318	9.04	40.49	38.65	1.03	47.31	
260-21	sphalerite		16.242	15.215	37.008	1295	9.06	40.16	39.86	1.77	45.85	
400-23	pyrite	pyrite-quartz vein	16.227	15.203	37.121	1294	9.04	40.76	38.83	1.02	49.01	
07SH-KSD-1	galena	massive poor ore	16.958	15.33	37.492	902	9.13	38.53	47.85	5.07	40.5	
07SH-KSD-2	galena		16.133	15.141	36.861	1299	8.92	39.42	33.23	-3.05	41.89	
K17	whole ore	ore	16.738	15.341	37.531	1071	9.2	40.42	49.71	7.43	49.64	Xi et al., 2008
K42	whole ore	ore	16.658	15.315	37.492	1101	9.17	40.54	47.49	6.04	49.99	
K100	whole ore	ore	16.669	15.345	37.484	1124	9.23	40.75	50.4	8.27	50.9	
A5	whole ore	ore	16.34	15.344	37.47	1354	9.32	43.35	52.03	11.1	61.86	Niu et al., 2002
	galena	silification rock	16.37	15.294	37.251	1284	9.2	41.33	46.92	6.85	52.16	Niu et al., 1994
	galena	quartz vein	16.121	15.274	37.01	1440	9.23	41.89	46.63	7.74	53.1	
YD1-P	galena	ore	16.337	15.332	37.438	1345	9.3	43.06	50.87	10.17	60.46	Yang et al., 1991
YD1-2	sphalerite	ore	16.178	15.139	36.843	1263	8.9	38.94	32.69	-3.63	39.65	
SZK25-1	pyrite	ore	16.162	15.134	36.825	1271	8.9	38.92	32.35	-3.84	39.5	
SZK2Q-4	pyrite	ore	16.525	15.329	37.44	1210	9.23	41.47	49.51	8.22	53.84	
SZK19-8	chloritization rock	alteration zone	16.42	15.298	37.435	1252	9.19	41.93	47.03	6.71	55.78	
SZK4-9	phyllic rock	alteration zone	16.293	15.137	38.878	1177	8.87	48.53	31.74	-4.79	92.66	
	granodiorite	plutonic rock	17.48	15.431	37.73	639	9.25	37.25	56.67	9.61	34.86	Yu et al., 1996
	quartz diorite porphyrite	plutonic rock	16.469	15.115	37.202	1023	8.78	38.29	28.47	-7.89	38.18	Niu et al., 2002
	porphyritic granite	plutonic rock	16.365	15.223	37.033	1215	9.04	39.41	39.91	1.31	42.66	Wang et al., 1995
	plagioclase amphibolite	host rock	16.278	15.007	36.738	1024	8.54	36	16.61	-16.29	25.26	Yu et al., 1996
	amphibole plagioclase geneiss	host rock	17.376	15.179	37.683	411	8.75	35.2	31.76	-8.26	23.36	
	biotite plagioclase geneiss	host rock	17.357	15.178	39.986	425	8.75	45.41	31.7	-8.25	87.76	
	granitic migmatite	host rock	15.821	15.122	38.234	1507	8.99	49.68	33.98	-1.24	91.41	

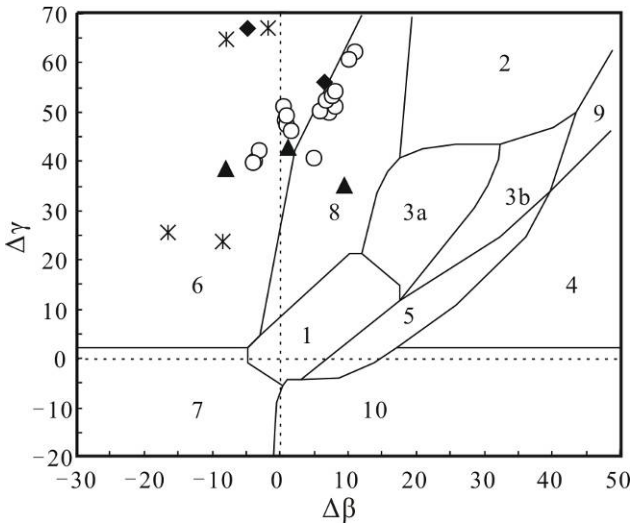

Figure 6. Δβ-Δγ genetic schematic diagram of the lead isotopes (after Zhu et al., 1998).
1-mantle-derived; 2-upper crust; 3-mantle and upper crust mixed subduction zone (3a-magmatism, 3b-sedimetation); 4-chemistry sediments; 5-hydrothermal sediments on the seafloor; 6-middle to deep metamorphism; 7-deep metamorphism lower crust; 8-orogenic belt; 9-upper crust of old shale; 10-retrogressive metamorphism.

5.2. Sulfur isotopes

The results of this and previous published studies of the sulfur isotopic compositions are presented in table 2. The $\delta^{34}S$ values of pyrite range from -0.4 to 5.0 ‰. Two samples of chalcopyrite yielded $\delta^{34}S$ values of 0.9 and 2.2 ‰. Sphalerite and galena yielded $\delta^{34}S$ values from 0.9 to 4.0 ‰ and from -2.2 to 1.6 ‰, respectively. Although there are some small differences between the $\delta^{34}S_{V\text{-}CDT}$ values of these minerals, those values are overlapping each other. The values of $\delta^{34}S$ are clustered in a small range of the +1.5~+2.5 ‰ and display a unimodal distribution, suggesting a sulfur reservoir dominated by magmatic or chondritic sulfur (Downes & Seccombe, 2008; Gülcan, 2009). This observation is consistent with the reduced nature of the assemblage (i.e., py-cpy-sp), which indicates the fluid was buffered to low values of SO_4: H_2S and that $^{34}S_{sulfide} \approx {}^{34}S_{H2S} \approx {}^{34}S_{fluid}$ (Ohmoto & Rye, 1979). Obvious tower effect showed by Fig. 7 illustrates that the homogenous sulfur isotope compositions have a single source for the different kinds of sulfide from the ores.

A sphalerite-chalcopyrite pair yielded $\delta^{34}S$ values of 3.0 and 2.2 ‰, respectively, for a $\Delta_{Sp\text{-}Cpy}$ value of 0.8 ‰, and pyrite-chalcopyrite pair yielded $\delta^{34}S$ values of 2.2 and 0.9 ‰, respectively, for a $\Delta_{Py\text{-}Cpy}$ value of 1.3 ‰. Therefore, the $\delta^{34}S$ value of the sphalerite-chalcopyrite and pyrite-chalcopyrite pairs from the same samples are in accordance with the expected fractionation trends of these mineral pairs. The sulfur-isotope geothermometric temperature values, calculated from the $\delta^{34}S$ values of these mineral pairs, are in a reasonable range, which is 160□ for sphalerite-chalcopyrite pair and 315□ for pyrite-chalcopyrite pair, respectively. These results indicate that these minerals did form in equilibrium. Therefore, the $\delta^{34}S_{V\text{-}CDT}$ values of H_2S in equilibrium with sulfides were estimated to be in the 0.9 to 3.0 ‰ with the average of 2.0 ‰ by evaluating the minimum and maximum $\delta^{34}S$ values of various sulfides. On the basis of geological and geochemical constraints, mineralization at the Shihu mine probably formed from moderate temperature (200-300 □), slightly acidic fluids at moderate fO_2 conditions. Under these conditions, gold is typically transported as a bisulfide complex [$Au(HS)^-_2$] (Hannington et al, 1999). Accordingly, gold deposition probably resulted from the mixing of reduced deep ore-forming fluids and with oxygenated infiltrated meteoric water because of the oxidation of $Au(HS)^-_2$.

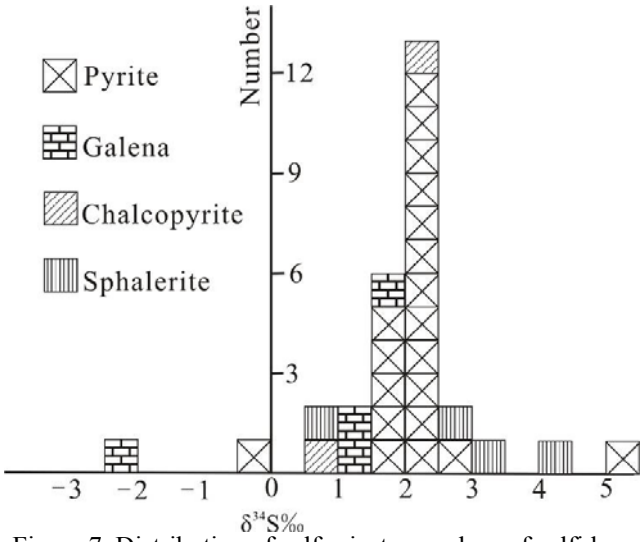

Figure 7. Distribution of sulfur isotope values of sulfides from the Shihu gold deposit

In addition, Iyer (1992) interpreted these lighter values of S isotope to reflect oxidation of reduced sulfur or influence of meteoric water resulting in increasing oxygen fugacity. For example, the upward pyrites decrease in $\delta^{34}S$ values, which are 2.35, 2.23, 2.19 and 1.99 ‰ corresponding to 180, 260, 400 and 560 meters level, respectively. The observations suggested that the altered rock type-gold deposit with heavier S values may be a next important prospecting direction in the deep area of Shihu mine.

5.3 Carbon and oxygen isotopes

The carbon and oxygen isotope compositions of veined calcite (3 samples) were analyzed. The results and previous studies are summarized in table 3. Vein calcite and auriferous vein quartz have $\delta^{18}O$ values ranging from 1.76 to 12.36 and 11.6 to 13.5 ‰ relative to SMOW, respectively. Calcite and quartz were deposited in near isotopic equilibrium with respect to $\delta^{18}O$, indicating fluid-dominated conditions during ore formation, from fluids of magmatic origin. However, the relatively large range in $\delta^{18}O$ values of calcite reflects, in part, low temperature exchange of carbonate with fluids (Shimazaki et al., 1986).

The $\delta^{13}C$ values for the carbonates indicate few depleted values, with the data falling between -4.29 and -6.92 ‰ relative to PDB, and intra deposit variability is small. These values are interpreted as the primary $\delta^{13}C$ signal of a mantle origin (Oberyhür et al., 1996). Given the dominance of CO_2 in the vein-forming fluids, based on the fluid inclusion studies, it can be assumed that $\delta^{13}C_{carb} \approx \delta^{13}C_{H2CO3} \approx \delta^{13}C_{fluid}$. The $\delta^{13}C$ value of the fluid is not due to in situ fractionation and the signal indicates a deep source of the carbon, which similarly coincides with the typically heavier values noted for other orogenic gold deposits (McCuaig & Kerrich, 1994). Thus, the $\delta^{13}C$ values indicate that the carbon was derived from the mantle, as was the sulfur.

Table 2. Sulfur isotopes compositions of pyrite, chalcopyrite, sphalerite and galena separated from different occurrences from the Shihu gold deposit

Sample no.	***Sample***	***Occurrence***	***$\delta^{34}S_{V\text{-}CDT}$‰***	***Reference***
560-13	pyrite	pyrite-quartz vein	-0.4	This study
400-23	pyrite	pyrite-quartz vein	1.7	
220-9	pyrite	pyrite-quartz vein	2.2	
180-9	chalcopyrite	polymetallic sulfide quartz vein	0.9	
300-25	chalcopyrite	polymetallic sulfide quartz vein	2.2	
260-21	sphalerite	polymetallic sulfide quartz vein	3	
07SH-KSD-1	galena	massive poor ore	1.1	
07SH-KSD-2	galena	massive poor ore	1.3	
R1	pyrite	480m level	2.2	Xi et al., 2008
R2	pyrite	300m level	2.2	
R3	pyrite	360m level	2.4	
R4	pyrite	220m level	2.4	
R5	galena	220m level	-2.2	
SYD-1	pyrite	polymetallic sulfide quartz vein	2.4	Cui et al., 1993
SZK13-3	pyrite	pyrite phyllic rock	1.7	
SYD2-3	pyrite	pyrite chloritization rock	2	
Td1-4	pyrite	pyrite-quartz vein	2.1	
Gd1-11	pyrite	pyrite-quartz vein	1.9	
SZK-49	pyrite	pyrite-quartz vein	5	Yang et al., 1991
SYD2Q-4	pyrite	pyrite chloritization rock	2.1	
SYD3Q-3-P	pyrite	disseminated poor ore	2.2	
TYD22-1	pyrite	disseminated poor ore	2.4	
B116-1-F	pyrite	disseminated poor ore	2.5	
SZK50-7	pyrite	polymetallic sulfide quartz vein	1.7	
SZK33-3-1	pyrite	polymetallic sulfide quartz vein	2.5	
YD1-F	pyrite	polymetallic sulfide quartz vein	2.8	
YD1-P	sphalerite	polymetallic sulfide quartz vein	0.9	
SYD3Q-3-Z	sphalerite	disseminated poor ore	4	
SYD2Q-3	sphalerite	carbonatization quartz vein	2.8	
SZK33-3	galena	polymetallic sulfide quartz vein	1.6	

Table 3. Carbon and oxygen isotopes compositions of calcite and dolomite from the Shihu gold deposit

Sample no.	*Sample*	$\delta^{13}C_{PDB}$ ‰	$\delta^{18}O_{PDB}$ ‰	$\delta^{18}O_{SMOW}$ ‰	*Reference*
SH-01	calcite	-6.92	-17.95	12.36	This study
SH-02	calcite	-5.95	-20.57	9.66	
SH-03	calcite	-5.93	-21.39	8.81	
STC550-1	calcite	-5.903	-28.227	1.76	Yang, et al., 1991
C102-2	calcite	-4.656	-24.628	5.47	
SZK20-4	calcite	-4.32	-25.18	4.90	
SZK18-6	calcite	-4.53	-25.15	4.93	
SZK15-7	calcite	-4.29	-24.46	5.65	
SYO_2Q	dolomite	-5.764	-18.087	12.21	

5.4. Hydrogen and oxygen isotopes

The δD values were analyzed directly from fluid inclusions in auriferous vein quartz. The $\delta^{18}O_{H2O}$ values were calculated from $\delta^{18}O$ of quartz using the formula: $1000\ln\alpha_{quartz\text{-}water}=3.38\times10^6/T^2-3.4$ (Taylor, 1974). The fluid inclusions in seven samples of quartz have similar δD and $\delta^{18}O_{H2O}$ values with respect to SMOW. The results are listed in table 4.

The δD values obtained from fluid inclusions in quartz can accurately reflect the δD values of the hydrothermal fluid (Faure, 2003). The δD values of vein quartz are in distinguishable and have a narrow range of –101 to –91 per mil. Using the formula reported by Taylor (1974), the $\delta^{18}O_{H2O}$ values calculated from $\delta^{18}O$ values of quartz range from 2.21 to 7.05 per mil at mean temperature of homogenization temperatures of fluid inclusions (Table 4). In the plot of δD vs. $\delta^{18}O$ (Fig. 8), seven quartz samples locate between the magmatic water field and the meteoric line. Similar to the coeval and co-genetic Taihangshan deposit from the same craton (Zhu et al., 2001), the ore-forming fluid in the Shihu Au deposit may be a mixture of meteoric water and magmatic water. Magmatic components and evolved meteoric waters for the fluid source for these types of deposits have also been proposed for the amphibolites or high amphibolites facies deposits (Yao et al., 1999; Fan et al., 2003).

The late Mesozoic age of mineralization at Shihu is about 2.0 Ga later than the age of metamorphism in the basement rocks. Instead, the close temporal and spatial association between mineralization zones and the Yanshanian granitoids suggests that deep-crustal granitic devolatilization would have generated the mineralizing fluids. Such genetic association between magmas and hydrothermal ore deposits has been documented in scores of geological studies of mineralization close to magmatic intrusions (Batchelder, 1977; Miao et al., 2002, 2003; Zhang et al., 2005). Deeply-circulating meteoric waters seem to be another likely fluid source for the Shihu deposit, as downward-percolating meteoric water is commonly reported to be a saline, aqueous fluid (Garba & Akande, 1992), which is similar to the late aqueous fluid in the Shihu deposit.

5.5. Strontium isotopes

Rb (0.38-113.50 μg/g) and Sr (2.00-41.41μg/g) for quartz and Rb (0.02-0.06 μg/g) and Sr (0.11-0.38μg/g) for pyrite are variable (Table 5). To determine whether the original $^{87}Sr/^{86}Sr$ values changed significantly and not due to ^{87}Rb decay since the ores were formed, the initial strontium isotope compositions of quartz and pyrite are calculated using the formula: $(^{87}Sr/^{86}Sr)_0 = {}^{87}Sr/^{86}Sr - {}^{87}Rb/^{86}Sr\,(e^{\lambda t}-1)$, $\lambda = 1.42\times10^{-11}\cdot a^{-1}$ and t = 130 Ma (unpublished zircon U-Pb data). The $(^{87}Sr/^{86}Sr)_0$ values of quartz range from 0.714057 to 0.825903 with mean value of 0.729604 and the values of pyrite range from 0.71345 to 0.723227 with mean value of 0.719663. The initial $^{87}Sr/^{86}Sr$ values of plutonic rocks are ranging from 0.7059 to 0.7068 (Yu et al., 1996). The initial $^{87}Sr/^{86}Sr$ values of Precambrian metamorphic basement are ranging from 0.7757 to 1.0641 with mean value of 0.8721 (Liu et al., 2000).

Rb and Sr in quartz and pyrite are concentrated in their fluid inclusion, so the characteristics of Rb and Sr in quartz and pyrite should represent the characteristics of hydrothermal fluid. The initial $^{87}Sr/^{86}Sr$ values of the host rocks in contact with the orebody are lighter than that of fresh host rocks. When the ore fluid passed through the host rocks, it might be altered by ore fluid, suggesting that the ore fluid included in quartz and pyrite must have lower $^{87}Sr/^{86}Sr$ values, which were from deep mantle-derived fluid (Mao et al., 2003; Zhai et al., 2001, 2003) reacted with the wall rocks.

Table 4. Hydrogen and oxygen isotopes compositions of quartz from the Shihu gold deposit

Sample no.	*Homogenization temperature□^{0}C□*	δD_{H2O} ‰	$\delta^{18}O_{SMOW}$ ‰	$\delta^{18}O_{H2O}$ ‰
300-17	376.39	-94	11.6	6.98
180-15	355.93	-99	12.2	7.05
180-7	339.89	-101	11.6	6.00
180-5	326.00	-97	12.1	6.08
300-25	271.50	-92	12.5	4.50
220-9	242.71	-99	12.1	2.79
180-9	206.65	-91	13.5	2.21

Table 5. Sr isotope data of the quartz and pyrite from the Shihu gold deposit

Sample no.	mineral	Rb (μg/g)	Sr (μg/g)	$^{87}Rb/^{86}Sr$	$^{87}Sr/^{86}Sr$	2σ	$(^{87}Sr/^{86}Sr)_0$
SH1	quartz	113.50	41.41	7.9493	0.728745	7	0.714057
SH2		2.26	2.60	2.5121	0.723277	9	0.718635
SH3		5.86	2.96	5.7500	0.7282783	8	0.717654
SH4		1.31	2.58	1.4786	0.7177054	7	0.714973
SH5		47.79	4.60	30.3212	0.7913097	7	0.735285
SH6		0.99	2.19	1.3139	0.7185895	6	0.716162
SH7		15.45	3.91	11.4808	0.7510663	8	0.729853
SH8		13.84	7.59	5.2914	0.7372598	7	0.727483
SH9		0.38	2.00	0.5455	0.7183771	9	0.717369
SH10		19.91	18.19	3.1734	0.7251153	5	0.719252
SH11		7.68	5.25	4.2428	0.7264572	6	0.718618
SH12		7.74	10.73	2.1125	0.8298059	7	0.825903
SH220-1	pyrite	0.05	0.33	0.4463	0.724051	29	0.723227
SH220-2		0.03	0.37	0.2186	0.720595	36	0.720191
SH220-3		0.02	0.21	0.2739	0.721837	58	0.721331
SH220-4		0.04	0.21	0.5888	0.722492	72	0.721404
SH220-5		0.04	0.11	1.2078	0.722916	36	0.720684
SH220-6		0.05	0.23	0.5705	0.719923	50	0.718869
SH220-7		0.06	0.38	0.4879	0.719052	22	0.71815
SH220-8		0.03	0.14	0.6611	0.714671	32	0.71345
97165-1	fine-grain adamellite	155.354	33.655	13.8266	1.08968	38	1.06413
97156-3	magnetite adamellite	102.783	40.65	7.4558	0.924589	20	0.91081
91758-2	coarse-grain adamellite	186.601	75.978	7.23588	0.915776	28	0.90241
97129-1	gneissic fine-grain adamellite	163.327	140.541	3.38668	0.802414	16	0.79616
97156-1	fine-grain biotite adamellite	143.798	152.954	2.73606	0.788452	21	0.78340
97145-2	two mica adamellite	159.112	193.005	2.39726	0.780115	23	0.77569

Note: $^{87}Sr_0/^{86}Sr_0$ was calculated using t=130 Ma. Errors: $n\times10^{-6}$. The data of adamellites are quoted from Liu et al. (2000).

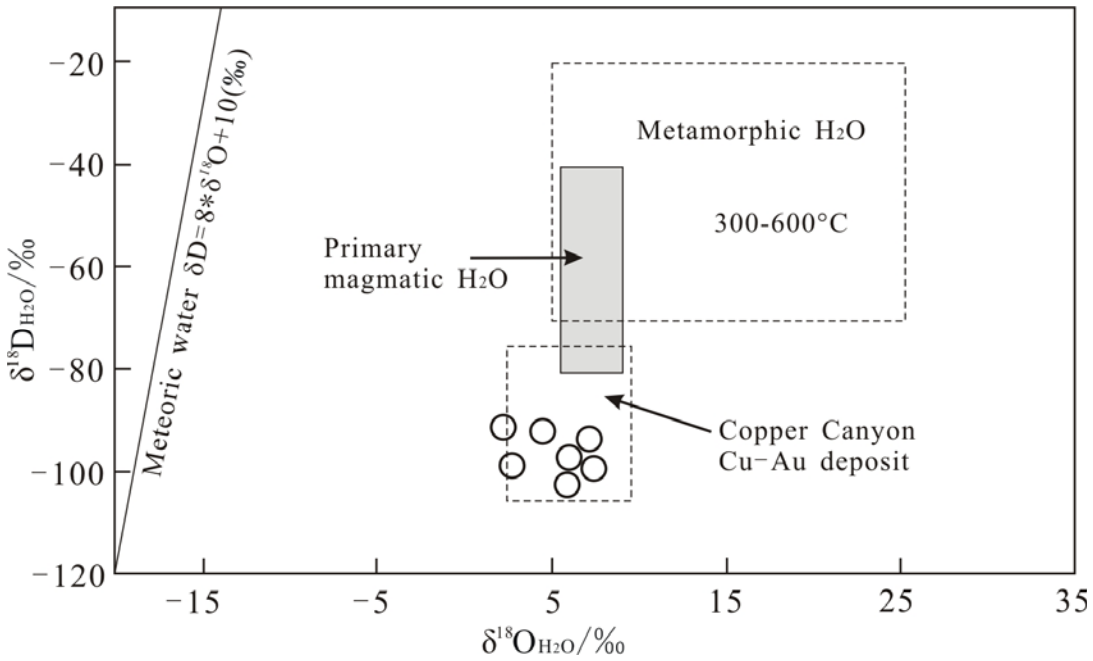

Figure 8. Plot of δD for aqueous fluids extracted from quartz vs. $\delta^{18}O$ of the fluids calculated from $\delta^{18}O$ of the host quartz. δD and $\delta^{18}O$ in per mil relative to SMOW. Open circles=Shihu mine. Canyon Cu-Au deposit are quoted from Batchelder (1977).

6. CONCLUSIONS

Mixture of upper mantle and lower crustal sources are the lead reservoirs for the Shihu deposit. Sulfides and host rocks have similar Pb isotope compositions. Lead isotope systematics show that the ore-forming materials derived from Precambrian wall rocks in underplating of the basaltic magmas in the lower crust.

The lighter values of $\delta^{34}S$ display a unimodal distribution, indicating that isotopic equilibrium among sulfides was attained and suggesting a sulfur reservoir dominated by magmatic or chondritic sulfur with the involvement of some sulfur of lighter isotopic composition. The S-isotope geothermometric value calculated from the mineral pairs are ranging 160□ to 315□.

Carbon and oxygen isotope studies suggest the ore fluid was magmatic origin without in situ fractionation, and a deep source of the carbon passed through the strata and reacted with wall rocks when it moved up to the site of ore deposition.

Hydrogen and oxygen isotope data of the fluid inclusions suggest that the ore fluid would be a mixture of meteoric water and magmatic water.

Strontium isotope study indicates that ore fluid is deep-seated mantle brine, with low $^{87}Sr/^{86}Sr$ value. On its pathway to site of ore deposition, it obtained its high Sr-isotope values from the Precambrian wall rocks.

These data comprehensively suggest that the ore-forming materials were leached out from the Precambrian basement, which was reacted with a mixing fluid are composed of deep-crustal granitic devolatilization, deep mantle-derived fluid and deeply-circulating meteoric waters.

ACKNOWLEDGEMENTS

This research is funded by National Natural Science Foundation Major Research Plan Key Support Project (Grant No. 90914002), and the 111 Project under the Ministry of Education and the State Administration of Foreign Experts Affairs, China (Grant No. B07011). We would like to acknowledge the support of the special funds from National Crisis Resources Prospecting Mining project management office. Thanks also to Wang Wenxue secretary of Shijiazhuang Comprehensive Geological Brigade and other colleagues of the Shihu Gold Deposit Company for their enthusiastic help with field work. We are very grateful to an anonymous referee who reviewed our manuscript with very constructive comments that greatly improved it.

REFERENCE

Andras, P., Chovan, M., Dirner, V., Kral, J., Bachlinski, R., 2010. *Pb-isotope study in Sb-mineralization from western Carpathian (Slovakia).* Carpathian Journal of Earth and Environmental Sciences, 5(2), 71-80.

Ault, K. M., and Williams -J., 2004. *Sulfur and lead isotope study of the EL Mochito Zn-Pb-Ag deposit*. Economic Geology, 99, 1223-1231.

Batchelder, J., 1977. *Light stable isotope and fluid*

inclusion study of the porphyry Cu deposit at Copper Canyon, Nevada. Economic Geology, 72, 60-70.

Cao, Y., Li, S. R., Zhang, H. F., Ao, C., Li, Z. Z. & Liu, X. B., 2010. *Laser probe $^{40}Ar/^{39}Ar$ dating for quartz from auriferous quartz veins in the Shihu gold deposit, western Hebei Province, North China*. Chinese Journal of Geochemistry, 29(4), 438-445.

Cao, Y., Li, S. R., Zhang, H. F., Liu, X. B., Li, Z. Z., Ao, C. & Yao, M. J., 2011. *Significance of zircon trace element geochemistry, Shihu gold mine, western Hebei province, North China*. Journal of Rare Earths, 29(3), 277-286.

Carr, G. R., Dean, J. A., Suppel, D. W. and Heithersay, P. S., 1995. *Precise lead isotope fingerprinting of hydrothermal activity associated with Ordovician to Carboniferous metallogenic events in the Lachlan Fold Belt of New South Wales*. Economic Geology, 90, 1467-1505.

Chen, B. and Zhai, M. G., 2003. *Geochemistry of late Mesozoic lamprophyre dykes from the Taihang Mountains, north China, and implications for the sub-continental lithospheric mantle*. Geological Magazine, 140(1), 87-93.

Chen, B., Tian, W., Zhai, M.G., & Arakawa, Y., 2005. *Zircon U-Pb geochronology and geochemistry of Mesozoic magmatism in the Taihang Mountains and other places of the North China Craton, with implications for petrogenesis and geodynamic setting*. Acta Petrologica Sinica, 21, 13-24 (in Chinese with English Abstract).

Chen, B., Tian, W., Jahn, B. M. & Chen, Z. C., 2008. *Zircon SHRIMP U–Pb ages and in-situ Hf isotopic analysis for the Mesozoic intrusions in South Taihang, North China craton: Evidence for hybridization between mantle-derived magmas and crustal components*. LITHOS, 102, 118-137.

Clayton, R.N., O'Neil, J.R. & Mayeda, T.K., 1972. *Oxygen isotope exchange between quartz and water*. Journal of Geophysical Research, 77, 3057-3067.

Coleman, M. L., Sheppard, T. J., Durham, J. J., Rouse, J. E. & Moore, G. R., 1982. *Reduction of water with zinc for hydrogen isotope analysis*. Analytical Chemistry, 54, 993-995.

Constantina, C., Szakacs, A. & Pecskay, Z., 2009. *Petrography, geochemistry and age of volcanic rocks in the Gurasada area, southern apuseni MTS.* Carpathian Journal of Earth and Environmental Sciences, 4(1), 31-47.

Cui, Y. H., 1993. *Chemical composition of pyrite from the Tuling-Shihu gold district and its genetic significance*. Acta petrologica et mineralogical, 12(4), 371-381 (in Chinese with English abstract).

Doe, B. & Stacey, J. S., 1974. *The application of lead isotopes to the problems of ore genesis and ore prospected evaluation. A. review*. Economic geology, 69, 757-776.

Downes, P. M. & Seccombe, G. R., 2008. *Sulfur-and lead-isotope signatures of orogenic gold mineralization associated with the Hill End Trough, Lachlan Orogen, New South Wales, Australia*. Mineralogy and Petrology, 94, 151-173.

Fan, H., Zhai, M., Xie, Y. & Yang, J., 2003. *Ore-forming fluids associated with granite-hosted gold mineralization at the Sanshandao deposit, Jiaodong gold province, China*. Mineralium Deposita, 38, 739-750.

Faure, K., 2003. *δD values of fluid inclusion water in quartz and calcite ejecta from active geothermal systems: Do values reflect those of original hydrothermal water?*. Economic Geology, 98, 657-660.

Garba, I. & Akande, S.L., 1992. *The origin and significance of non-aqueous CO_2 fluid inclusions in the auriferous veins of Bin Yauri, north-western Nigeria*. Mineralium Deposita, 27, 249-255.

Glesemann, A., Jäger, H-J., Norman, A. L., Krouse, H. R. & Brand, W. A., 1994. *On-line sulfur-isotope determination using an elemental analyser coupled to a mass spectrometer*. Analytical Chemistry, 66(18), 2816-2819.

Gulson, B. L., Korsch, M. J., Cameron, M., Vaasjoki, M., Mizon, K. J., Porritt, P. M., Carr, G. R., Kamper, C., Dean, J. A. & Calvez, J. -Y., 1984. *Lead isotope ratio measurements using the Isomass 54E in fully automated mode*. International Journal of Mass Spectrometry, 59, 125–142.

Gülcan, B., 2009. *Sulfur- and lead-isotope geochemistry of the Arapuçandere lead-zinc-copper deposit, Biga Peninsula, northwest Turkey*. International Geology Review, 52, 1-14.

Hannington, M., Herzig, P., Scott, S., Thompson, G. & Rona, P., 1999. *Comparative mineralogy and geochemistry of gold-bearing sulfide deposits on the mid-ocean ridges*. Marine Geology, 101, 217-248.

Hoefs, J., 1997. *Stable Isotope Geochemistry*. 4th ed., Springer-Verlag, Berlin, 201 pp.

Iyer, S. S., 1992. *Sulfur and lead isotope geochemistry of galenas from the Bambui group, mines gerais— implications for ore genesis*. Economic Geology, 87, 437-443.

Li, S.G., Xiao, Y.L., Liou, D.L., Chen, Y.Z., Ge, N.J., Zhang, Z.Q. & Sun, S.-S., 1993. *Collision of the North China and Yangtze Blocks and formation of coecite-bearing eclogites: timing and processes*. Chemical Geology, 109, 98-111.

Liu, S. W., 1997. *Study on fluid-rock equilibrium systems of Fuping gneiss complex, TaihangMountains*. Science in China, Ser D, 40, 239-248.

Liu, S. W., Liang, H. H., Zhao, G. C., Hua, Y. G. & Jian, A. H., 2000. *Isotopic chronology and geological events of Precambrian complex in Taihangshan region*. Science in China, Ser D, 43, 386-393.

Liu, S. W., Pan, Y. M., Xie, Q. L., Zhang, J. & Li, Q. G., 2004. *Archean geodynamics in the Central Zone, North China Craton: constraints from geochemistry of two contrasting series of*

granitoids in the Fuping and Wutai complexes. Precambrian Research, 130, 229-249.

Ma, X.Y., Liu, G. & Su, J., 1984. *The structure and dynamics of the continental lithosphere in north – northeast China*. Annals of Geophysics, 2, 611–620.

Mao, J. W., Zhang, Z. H., Yu, J. J. & Niu, B. G., 2003. *Geodynamic settings of Mesozoic large-scale mineralization in North China and adjacent areas——Implication from the highly precise and accurate ages of metal deposits*. Science in China, Ser D, 46, 289-299.

McCrea, J. M., 1950. *On the isotopic chemistry of carbonates and a paleotemperature scale*. Journal of Chemical Physics, 18, 849–859.

McCuaig, T.C. & Kerrich, R., 1994. *P-T-t-deformation-fluid characteristics of lode gold deposits*. in, Lentz, D., ed., *Alteration and Alteration Processes Associated with Ore-forming Systems*, Geological Association Canada Mineralogical Association Canada, Short Course Notes, 11, 339-380pp.

Menzies, M., Xu, Y. G., Zhang, H. F. & Fan, W. M., 2007. *Integration of geology, geophysics and geochemistry: A key to understanding the North China Craton*. Lithos, 96, 1-21.

Miao, L. C., Qiu, Y. M., McNaughton, N. J., Luo, Z. K., Groves, D. I., Zhai, Y. S., Fan, W. M., Zhai, M. G., & Guan, K., 2002. *SHRIMP U-Pb zircon geochronology of granitoids from Dongping Area, Hebei Province, China: Constraints on tectonic evolution and geodynamic setting for gold metallogeny*. Ore Geology Reviews, 19, 187-204.

Miao, L. C., Qiu, Y. M., McNaughton, N. J., Fan, W. M., Groves, D. & Zhai, M. G., 2003. *SHRIMP U-Pb zircon ages of granitoids in the Wulashan gold deposit, Inner Mongolia, China: timing of mineralization and tectonic implications*. International geology review, 45, 548-562.

Niu, S. Y., Chen, L. & Xu, C. S., 1994. *Crustal evolution and metallogenic regularity in the Taihang Mountains*. Beijing: Earthquake publishing house (in Chinese with English abstract).

Niu, S. Y., Li, H. Y., Sun, A. Q., Wang, B. D., Xu, C. S., Xie, R. B., Yang, Z. H. & Bi, F. K., 2002. *Mantle Branch Structure Theory and Exploration Practice*. Beijing: Seismological Press (in Chinese with English abstract).

Oberyhür, T., Mumm, A. S., Vetter, U., Simon, K. & Amamor, J. A., 1996. *Gold mineralization in the Ashanti belt of Ghana: Genetic constraint of the stable isotope geochemistry*. Economic geology, 91, 289-301.

Ohmoto, H., & Rye, R.O., 1979. *Isotopes of Sulfur and Carbon*, in **Barnes, H.L.,** ed. *Geochemistry of Hydrothermal Ore Deposits*, J. Wiley & Sons, New York, 509-567.

Peng, Q. M. & Xu, H., 1994. *The discovery of native ruthenium in Nuanquanzi and Tuling-Shihu gold deposits: Implications for Source of Gold*. Chinese Journal of Geochemistry, 13, 123-131.

Qiao, G. S., 1988. *Normalization of isotopic dilution analysis—A new program for isotope mass spectrometric analysis*. Scientia Sinica, ser. A, 31, 1263-1268.

Robert R. Seal II, Robert A. A., Nora K. F. & Sandra H. B., 2001. *Sulfur and lead isotope geochemistry of hypogene mineralization at the Barite Hill Gold Deposit,Carolina Slate Belt, southeastern United States: a window into and through regional metamorphism*. Mineralium Deposita, 36, 137-148.

Shimazaki, H., Shimizu, M. & Nakano, T., 1986. *Carbon and oxygen isotope of calcite from Japanese skarn deposit*. Geochemical Journal, 20, 297-310.

Tang, Y. J., Zhang, H. F. & Ying, J. F., 2006. *Asthenosphere–lithospheric mantle interaction in an extensional regime: Implication from the geochemistry of Cenozoic basalts from Taihang Mountains, North China Craton*. Chemical Geology, 233, 309-327.

Taylor, H. P. Jr., 1974. *The application of the oxygen and hydrogen isotope studies to problems of hydrothermal alteration and ore deposition*. Economic Geology, 69, 843-883.

Yang, J. H. & Zhou, X. H., 2001. *Rb-Sr, Sm-Nd, and Pb isotope systematics of pyrite: Implications for the age and genesis of lode gold deposits*. Geology, 29, 711-714.

Yang, D. F., Li, G. S., Jia, K. S., Wang, X. C., Ju, G. & Wang, J. S., 1991. *Study on the ore-forming conditions and genesis of Tuling and Shihu gold gold deposit in the Taihang Mountain region.* Journal of Changchun University of earth science, 21(1), 45-53 (in Chinese with English abstract).

Yao, Y., Morteani, G. & Trumbell, R.B., 1999. *Fluid inclusions microthermometry and the P–T evolution of gold-bearing hydrothermal fluids in the Niuxinshan gold deposit, eastern Hebei Province, NE China*. Mineralium Deposita, 34, 348-365.

Yu, X. H., Ren, J. Y. & Zhang, J. X., 1996. *Cu-Au metallogenic condition and prospecting direction in the middle section of Taihang Mountains*. Beijing, Geological Publishing House (in Chinese).

Xi, C. Z., Dai, T. G., Liu, W. & Zhang, H. J., 2008. *Petrogeochemical characteristics of the intrusive bodies of Mapeng granitoids in western Hebei*. Acta Petrologica et Mineralogica, 27(2), 113-120 (in Chinese with English abstract).

Xi, C. Z., Dai, T. G. & Liu, W., 2008. *Geological-Geochemical Characteristics of the Shihu Gold Deposit in Western Hebei Province*. Acta Geoscientica Sinica, 29(4), 451-458 (in Chinese with English abstract).

Yang, J. H., Wu, F. Y. & Wilde, S. A., 2003. *A review of the geodynamic setting of large-scale Late Mesozoic gold mineralization in the North China Craton: an association with lithospheric thinning*. Ore geology reviews, 23, 125-152.

Wang J S, Tian B L. & Li C L., 1990. *Geological*

exploration report on the middle section of Tuling-Shihu gold mining area, 520 Team of first Geological Exploration Bureau of Ministry of Metallurgical Industry (in Chinese).

Zartman, R. E. & Haines, S. M., 1988. *The plumbotectonic model for Pb isotopic systematics among major terrestrial reservoirs–A case for bi-directional transport*. Geochimica et Cosmochimica Acta, 52, 1327-1339.

Zhai, M. G., Yang, J. H. & Liu, W. J., 2001. *Large clusters of gold deposits and large-scale metallogenesis in the Jiaodong Peninsula, Eastern China*. Science in China, Ser D, 44: 545-552.

Zhai, M. G., Zhu, R. X., Liu, J. M., Meng, Q. R., Hou, Q. L., Hu, S. B., Li, Z., Zhang, H. F. & Li, W., 2003. *Time range of Mesozoic tectonic regime inversion in eastern North China Block*. Science in China, Ser D, 46, 913-919.

Zhao, G. C., Cawood, P.A., Wilde, S.A., Sun, M. & Lu, L.Z., 2000. *Metamorphism of basement rocks in the Central Zone of the North China Craton: implications for Paleoproterozoic tectonic evolution*. Precambrian Research, 103, 55-88.

Zhai, M. G., Yang, J. H., Fan, H. R., Miao, L. C. & Li, Y. G., 2002. *A large-scale cluster of gold deposits and metallogenesis in the eastern North China craton*. International geology review, 44, 458-476.

Zhang, X. H., Liu, Q., Ma, Y. J. & Wang, H., 2005. *Geology, fluid inclusions, isotope geochemistry, and geochronology of the Paishanlou shear zone-hosted Gold Deposit, North China Craton*. Ore Geology Reviews, 26, 325–348.

Zhu, B. Q., 1995. *The mapping of geochemical provinces in China based on Pb isotopes*. Journal of geochemical exploration, 55, 171-181.

Zhu, B. Q., 1998. *Isotopic systematic theory and application in earth science: Concurrently discussing crust-mantle evolution of Chinese continent*. Beijing: Science Press, 330 pp (in Chinese with English abstract).

Zhu, Y. F., Zeng, Y. S. & Jiang, N., 2001. *Geochemistry of the Ore-Forming Fluids in Gold Deposits from the Taihang Mountains, Northern China*. International Geology Review, 43, 457-473.

Received at: 22. 02. 2011
Revised at: 09. 04. 2011
Accepted for publication at: 15. 05. 2011
Published online at: 30. 05. 2011